Distributed Electric Powertrain Test Bench With Dynamic Load Controlled by Neuron PI Speed-Tracking Method

Wanbang Zhao, Qiang Song🆔, Wenbin Liu, Mukhtiar Ahmad, and Yiting Li

Abstract—Based on the real-time model and platform, a dynamic hardware-in-the-loop (HIL) testing method for the distributed powertrain of electric vehicle (EV) is proposed. Compared with static point testing, the dynamic HIL test can provide a more realistic working environment for the EV's distributed electric powertrain (DEP) early development. The test data of electric motor's efficiency and maneuver performance under a dynamic work condition are more authentic and meaningful. Meanwhile, the driver-vehicle-road real-time (DVRRT) model is set up to emulate the actual condition. The speed-tracking control method with proportional–integral (PI) gains tuned by the neuron network algorithm is used to generate the distributed real-time loads. Maximum adhesion limitation is added once the slipping is detected in the real-time model. Simulation and experiment of the test bench are done. The generated distributed load is compared with both the theoretical one and the simulated one in the Carsim software platform. Two comparisons show the similar results. The load accuracy is high, but there is a short time delay. The mechanical work measured by the experiment test bench is highly consistent (97.5%) with the theoretical value. As a result, the proposed test bench and its control method can be used for DEP efficiency test.

Index Terms—Distributed electric powertrain (DEP), driver-vehicle-road real-time (DVRRT) model, dynamic loading, dynamometer, hardware-in-the-loop (HIL) test bench.

I. Introduction

WITH the draining of the fossil resources and the heavy air pollution in the urban cities, the emission-free vehicle seems to be a perfect solution. Researches on electric vehicle (EV) technology are done by many engineers. Due to the flexible layout of the electric motors compared with combustion engines, some new types of powertrain structure for EV have been proposed such as hybrid powertrain [1], dual-motor coupling powertrain [2], powertrain with two propulsion machines, and a torque coupler [3], while distributed electric powertrain (DEP) is a unique one, in which every driving wheel is equipped with an independent powertrain. Various control strategies are proposed to improve the dynamic performance in steering maneuvers and energy consumption

efficiency of DEP, such as [4]–[7]. Zhuoping *et al.* [8] summarize the features and existing dynamics control strategies of DEP.

Bilgin *et al.* [9] state "In electrified powertrain applications, the efficiency of the electrical path, and the power and energy density of the components play important roles." But it is hard to test DEPs' efficiency and dynamic performance on the test bench except the real road test. The traditional test facilities such as dynamometers without a dynamic control strategy can only test the static torque characteristics with static load [10]. However, the electric motors of vehicle are different from the other industrial electric motors; the work condition covers a large range. The static point test cannot reflect the realistic efficiency and dynamic performance of the tested motors under its unique work condition. Newton *et al.* [11] bring up the idea to emulate dynamic load characteristics with a dynamic dynamometer. This paper also proposed a hardware-in-the-loop (HIL) dynamic test equipment and the method for vehicle. There are several methods to generate the dynamic load; the conventional one is inverse dynamics method. Ma *et al.* [12] take the road/tire longitudinal interaction into account and give the dynamometer, the torque order equal to the dynamic load. Test bench for emulating the electric-drive vehicle system is established by Fajri *et al.*'s [13], [14] team. Inertia equivalent, vehicle resistance, and friction braking are concerned when generating the dynamic load. However, those test bench cannot be directly used as a laboratory facility to test DEP. Multiple dynamometers are required to generate distributed load for each independent driving motor (DM) of the DEP.

This paper proposed a novel test bench control method to implement the DEP HIL dynamic test. A real-time model of the DEP vehicle and the test environment are established. The speed-tracking control is proposed to generate the dynamic distributed load, in which dynamometers' proportional–integral (PI) parameters are tuned by the neuron network algorithm. The maximum adhesion is also concerned in the control strategy. Test bench experiment and Carsim simulation comparison are shown in the last section.

II. Torque Distribution Strategies and Vehicle Dynamics of the DEP

A. DEP Vehicle Dynamics

For the distribute driving EV, it has the following characters. Its torque response is dramatically faster than the traditional
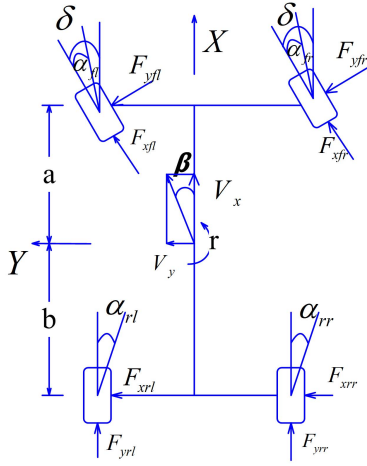
Fig. 1. Dynamics of the vehicle.

Fig. 2. Driving-force distribution strategies for DEP.

vehicle driven by the internal combustion engine. Each driving wheel has its independent electric powertrain which can be controlled individually. The differential torque output of the wheels on the same axle can generate a yaw moment defined as direct yaw-moment control. The dynamic control functions such as traction control and antilock braking are realized by the independent torque output on each driving wheel accurately and rapidly [5]. To simplify the problem and test bench structure, the DEP studied and tested in this paper is the one which has the dual-independent motors for steering axle (front axle).

For each independent driving wheel, there is an equation

$$I_{tw} \cdot \dot{w}_i = -R_w \cdot F_{xi} - T_{bi} + T_{di} \tag{1}$$

where I_{tw} is the rotational inertia of the wheel. w_i is the rotation speed of each wheel. T_{di} and T_{bi} are the driving and braking torques on it. R_w is the rotational radius. F_{xi}, F_{yi}, and F_{zi} mean the longitudinal, lateral, and vertical forces of each tire, respectively, in which i changes with the wheel (fl for front left, fr for front right, rl for rear left, and rr for rear right).

The DEP vehicle dynamics (shown in Fig. 1) can be summarized in the following equation, in which the longitudinal kinetics, lateral kinetics, and yaw kinetics are shown:

$$\begin{cases} m(\dot{V}_x - r \cdot V_y) = F_{xf} \cos \delta - F_{yf} \sin \delta + F_{xr} \\ m(\dot{V}_y + r \cdot V_x) = F_{xf} \sin \delta + F_{yf} \cos \delta + F_{yr} \\ I_z \cdot \dot{r} = (F_{xf} \sin \delta + F_{yf} \cos \delta)a \\ \quad + (\Delta F_{xf} \cos \delta + \Delta F_{yf} \sin \delta)\dfrac{t_{w1}}{2} + \Delta F_{xr}\dfrac{t_{w2}}{2} - F_{yr}b. \end{cases} \tag{2}$$

Axial load transfer due to acceleration is

$$\begin{cases} F_{zfl} = mg\dfrac{b}{2l} - m\dot{V}_x\dfrac{h_g}{2l} - m\dot{V}_y\dfrac{h_g}{t_{w1}} \cdot \dfrac{b}{l} \\ F_{zfr} = mg\dfrac{b}{2l} - m\dot{V}_x\dfrac{h_g}{2l} + m\dot{V}_y\dfrac{h_g}{t_{w1}} \cdot \dfrac{b}{l} \\ F_{zrl} = mg\dfrac{a}{2l} + m\dot{V}_x\dfrac{h_g}{2l} - m\dot{V}_y\dfrac{h_g}{t_{w2}} \cdot \dfrac{a}{l} \\ F_{zrr} = mg\dfrac{a}{2l} + m\dot{V}_x\dfrac{h_g}{2l} + m\dot{V}_y\dfrac{h_g}{t_{w2}} \cdot \dfrac{a}{l}. \end{cases} \tag{3}$$
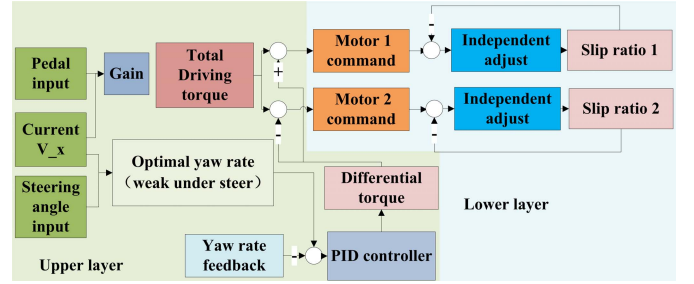
In (2) and (3), m is the mass of vehicle. I_z is the yaw rotational inertia. V_x and V_y are the longitudinal and lateral velocity. δ represents the steering angle of the front wheel (positive for left turn), α in shown in Fig. 1 is the slip angle of each tire, and r stands for the yaw rate. a and b are corresponding to the distance from the front axle to the center of gravity (CG) and from the rear axle to CG, and the wheelbase is $l = a + b$. Front and rear tracks are t_{w1} and t_{w2}. The axle total force value F_i and the differential values ΔF_i are calculated by the following equation:

$$\begin{cases} F_{xf} = F_{xfl} + F_{xfr} \quad F_{xr} = F_{xrl} + F_{xrr} \\ \Delta F_{xf} = F_{xfl} - F_{xfr} \quad \Delta F_{xr} = F_{xrl} - F_{xrr} \\ F_{yf} = F_{yfl} + F_{yfr} \quad F_{yr} = F_{yrl} + F_{yrr} \\ \Delta F_{yf} = F_{yfl} - F_{yfr} \quad \Delta F_{yr} = F_{yrl} - F_{yrr}. \end{cases} \tag{4}$$

Differential longitudinal force on each tire can generate the direct yaw moment M_d to assist the steering, and the traditional interwheel differential can be replaced. The process can be described in (5), in which the coaxial differential longitudinal tire force ΔF_{xi} is related to the distribution of the driving force. There are many distribution strategies to achieve the direct yaw-moment control and electric differential

$$M_d = \Delta F_{xf} \cos \delta \frac{t_{w1}}{2} + \Delta F_{xr} \frac{t_{w2}}{2}. \tag{5}$$

B. DEP Distribution Strategies

The leading researches [4], [15] propose a double-layer control structure, as shown in Fig. 2. The upper layer uses the optimal control and distributes the total driving torque demand to keep steering stability. The lower layer adjusts each independent powertrain torque output according to the observed slip ratio of each wheel to fulfill the antilock braking and antislid regulation function.

Some other distribution strategies focused on the energy conservation, using the minimal total energy consumption of the distributed electric motors as one of the optimal control objectives [6]. In this paper, the ground test is done to verify the proposed strategies. The DEP is equipped on a demonstrator vehicle first; then, the skid-pad test is done, as well as energy efficiency test on a rolling road with various driving cycles. But the ground test will extend the regression test period of control strategy and cost more money. A DEP HIL test bench, which generates the real-time distributed dynamic load, can accomplish a similar test.
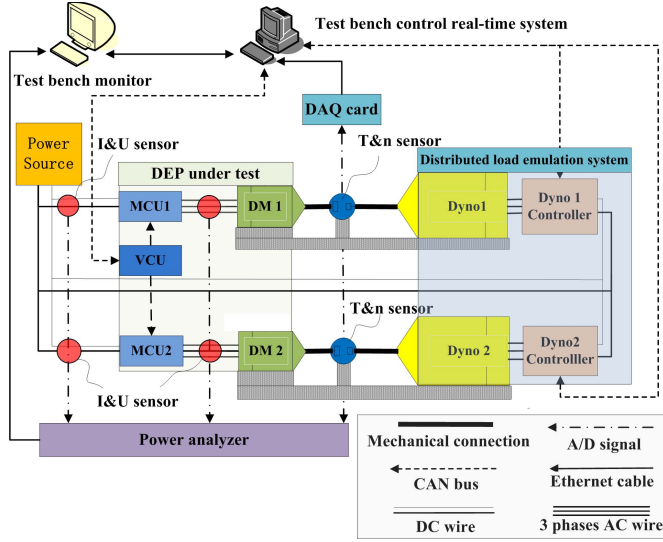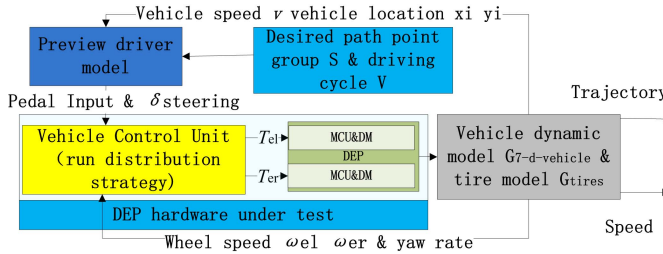
Fig. 3. Structure of the DEP test bench.

Fig. 4. DVRRT model.

III. TEST BENCH STRUCTURE AND REAL-TIME MODEL

A. Test Bench Structure

To achieve distributed load and illustrate the loading method, the structure of the DEP test bench as shown in Fig. 3 is introduced. There are four sections including DEP under test, distributed load emulation system, data acquisition system, and real-time control system. DEP contains two DMs equipped with motor control units (MCU) and vehicle control unit (VCU). Distributed load emulation system is used to generate the real-time distributed mechanical load, including two dynamometers and their controllers. The data acquisition system consists of torque and speed sensors, current and voltage sensors, power analyzer, and data acquisition system to get the test data online and return to the real-time system. The control system is a real-time platform of xPC. In Fig. 3, the host computer works as a test bench monitor whose functions are visualization of the sensor data and setting the driving cycle, desired path, and road condition. The target computer is the real-time control system which runs the real-time model.

B. Driver-Vehicle-Road Real-Time Model

To accomplish an HIL test, the real-time model is necessary. The driver-vehicle-road real-time (DVRRT) model is established to create a driving cycle, driver inputs, and road environment for DEP, as shown in Fig. 4, where the rotation speed of wheels are ω_{el} and ω_{er} and the distributed torque

commands are T_{el} and T_{er}. With the only hardware (DEP) in the loop, the real-time model is supposed to generate the driver's steering wheel angle $\delta_{steering}$ and pedal input based on the desired path and driving cycle, and emulate vehicle dynamics and tire-road interactions.

Unlike the ground test, the DEP is in the loop, and the VCU requires a virtual driver signal input to run the torque distribution algorithm online. A preview driver model (introduced in [16]) is established, in which the speed control adopts an antisaturated integral PID controller, and path tracing is achieved by the preview follow theory [17], [18].

1) Preview Driver Model: In this paper, only the electric braking is concerned, while ignoring the friction braking. The pedal input is a single value which combines the accelerating pedal value and the braking pedal value. The positive input represents the acceleration and the negative one for braking. The input value is calculated by the following equations:

$$T_r = \frac{mg\sin\theta + mg\cos\theta \cdot f + \left(\frac{C_D A}{21.15}v_x^2\right)_j + \delta m \frac{dv_x}{dt}}{R \cdot \eta \cdot G} \tag{6}$$

$$T_{error}(s) = E(s) \cdot G(s) = \left(K_p + \text{sat}\left(\frac{1}{T_i s}\right) + T_d s\right) \cdot E(s) \tag{7}$$

$$\text{Input} = \frac{T_{error} + T_r}{T_{max}} \tag{8}$$

where T_r is the overall resistance transmitted to the powertrain system. m is vehicle mass; g is gravity constant. O is road gradient. f is road rolling resistance coefficient. C_D is the air dynamic coefficient, 21.15 is a constant related to air density. A is the vehicle front area. v_x is vehicle longitudinal speed. δ is the mass coefficient after considering the rotational inertia. η is the powertrain mechanical coefficient. G is the gear ratio. R is the wheel rotational radius. K_p, T_i, and T_d are the parameters of the PID controller. The sat( ) means the saturation value. E is the speed error. $G(s)$ is the transfer function of the PID controller. T_{error} is the torque output of the PID controller. T_{max} is the maximum torque output capacity of the electric motor under current speed.

Under extreme conditions, the limitation of powertrain system's maximum output or tire-road adhesion can lead to a huge gap between the virtual speed and the reference speed [19], [20]. As a result, the integral section accumulates the error and overreacts, returning an unreasonable value which is different from a human driver's behavior. The saturation function sat( ) is introduced into the PID controller to solve this issue.

The driver model in the traditional HIL test bench for single powertrain EV does not contain a steering function. However, the steering maneuvers are a typical work condition for DEP, and steering wheel angle is also required by the distribution law. The steering function is inevitable for this driver model. Preview follow theory [17] is adopted to generate the appropriate steering angle which is briefly introduced in this paper (refer to [17] for more detail). The scan method is used to find the preview point shown in Fig. 5(a) [17]. T is the preview time. The driver model [Fig. 5(b)] calculates
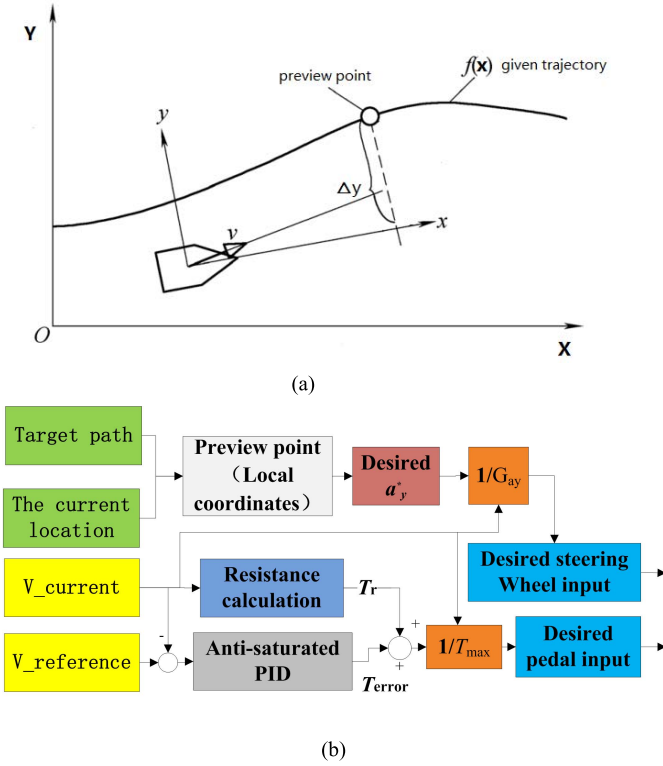
(a)

(b)

Fig. 5. Preview driver model. (a) Preview-follow theory. (b) Structure of the driver model's algorithm.

the desired acceleration in the y-direction (a_y^*) according to Δy, as

$$a_y^* = \frac{2}{T^2}(\Delta y - v_y T). \quad (9)$$

To get a weak understeer character, the steering gain is decided by

$$G_{ay} = \frac{V_x^2}{l + kV_x^2} \quad (10)$$

where l is the wheelbase. k is the understeer parameter ($k > 0$). The desired steering wheel angle input $\delta_{steering}$ is calculated as

$$\delta_{steering} = \frac{a_y^*}{G_{ay}} \cdot i_{steering} \quad (11)$$

where $i_{steering}$ is the steering ratio.

2) Vehicle Dynamics Model G7-d-Vehicle: The hardware is electric motors of DEP on the bench. The whole vehicle is a virtual model running in the real-time system. The longitudinal, lateral, and yaw motions of the vehicle body are shown in (2)–(5). The longitudinal speed of each wheel hub V_{wi} can be calculated as

$$\begin{cases} V_{wfl} = \left(V_x - \frac{t_{w1}}{2}r\right)\cos\delta + (V_y + ar)\sin\delta \\ V_{wfr} = \left(V_x + \frac{t_{w1}}{2}r\right)\cos\delta + (V_y + ar)\sin\delta \\ V_{wrl} = V_x - \frac{t_{w2}}{2}r \\ V_{wrr} = V_x + \frac{t_{w2}}{2}r. \end{cases} \quad (12)$$

The slip ratio of each wheel λ_i follows:

$$\lambda_i = \frac{w_i R - V_{wi}}{V_{wi}}. \quad (13)$$

3) Tire Model Gtires: Tire-road interactions are also contained in the model. The Dugoff tire model which is widely used as theoretical model is applied to the DVRRT model. It is simplified as

$$\begin{cases} \varphi_i = \dfrac{\mu F_{zi}(1 - \lambda_i)}{2\sqrt{(C_{xi}\lambda_i)^2 + (C_{yi}\tan\alpha_i)^2}} \\ f(\varphi_i) = \begin{cases} (2 - \varphi_i)\varphi_i & \varphi_i \le 1 \\ \varphi_i & \varphi_i > 1 \end{cases} \end{cases} \quad (14)$$

$$\begin{cases} F_{xi} = C_{xi}\dfrac{\lambda_i}{1 - \lambda_i}f(\varphi_i) \\ F_{yi} = C_{yi}\dfrac{\tan(\alpha_i)\lambda_i}{1 - \lambda_i}f(\varphi_i) \end{cases} \quad (15)$$

where λ_i is the tire slip ratio. C_{xi} is the tire longitudinal stiffness. C_{yi} is the cornering stiffness. φ_i is the active factor. The piecewise function $f(\varphi_i)$ is related to the active factor. Based on $f(\varphi_i)$, the longitudinal and lateral forces F_{xi} and F_{yi} of the tire can be calculated in (15).

IV. DYNAMIC DISTRIBUTED LOAD CONTROL METHOD

A. Theoretical Load of DEP

The conventional EV load on dynamometer consists of resistance T_R and inertia emulating $J_e\dot\omega$. Regarding the vehicle as 2 degree of freedom body, the kinetic energy E consists of the rotational parts and forward parts, as

$$E = \frac{1}{2}mv_x^2 + \frac{1}{2}\sum_{k=1}^{2}J_k\varpi_k^2 \quad \varpi_1 = \frac{v_x}{R_w} \quad \varpi_2 = G\varpi_1 \quad (16)$$

where J_k is the rotational inertia of each rolling parts on vehicle which rotation speed is ϖ_k. v_x is the longitudinal speed. ϖ_1 is the low rotation speed (wheel speed). ϖ_2 is the high rotation speed (motor speed), and G is the gear ratio.

The energy consumption of the dynamometer should be equal to the vehicle kinetic energy. The equivalent rotational inertia J_e is deduced by

$$\begin{cases} \dfrac{1}{2}J_e\varpi_2^2 = \dfrac{1}{2}mv_x^2 + \dfrac{1}{2}\sum_{k=1}^{2}J_k\varpi_k^2 \\ J_e = \dfrac{mR_w^2}{G^2} + \dfrac{J_1}{G^2} + J_2 \quad \varpi_2 = G\varpi_1 = G\dfrac{v_x}{R_w}. \end{cases} \quad (17)$$

The resistance force F_r is shown as

$$F_r = mg\sin\theta + mg\cos\theta \cdot f + \frac{C_D A}{21.15}v_x^2 + \delta m\frac{dv_x}{dt}. \quad (18)$$

According to (18), the resistance torque transmitted to the DEP is

$$T_R = \frac{F_R R_w}{\eta G}. \quad (19)$$

The total load of the two DEP dynamometers is calculated by

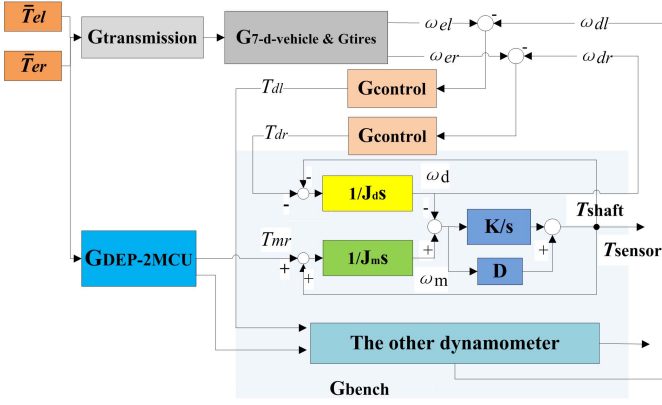$$T_d = j_e\dot\omega + T_R = T_{dl} + T_{dr} \quad (20)$$

Fig. 6. Speed-tracking method for test bench control.

Nevertheless, like the DEP distribution of driving torque, the load should also be distributed to the individual dynamometer (T_{dl} and T_{dr}). The distribution of load is related to the yaw motion. Simplified by (2), we get (21). The simplification is based on several assumptions and approximations. The two sideslip angles of the driving wheel are approximately the same. So, the lateral forces of the two front wheels are approximately equal to $F_{yfl} \approx F_{yfr}$

$$\eta G(T_{dr} - T_{dl})\frac{t_{w1}}{2R_w} = I_z \cdot \dot{r} - (F_{yfl} + F_{yfr})\cos\delta a \\ + (F_{yrl} + F_{yrr})b - (T \cdot R - F_r)\sin\delta a. \quad (21)$$

Combined (20) and (21), the load of the bilateral dynamometers should be distributed according to the following equation:

$$\begin{cases} T_{dr} = \frac{1}{2}\left(J_e\dot{\omega} + \frac{F_R R_w}{\eta G}\right) + \frac{R_w}{t_{w1}\eta G}(I_z \cdot \dot{r} - (F_{yfl} + F_{yfr}) \\ \quad \times \cos\delta a + (F_{yrl} + F_{yrr})b - (T \cdot R - F_r)\sin\delta a) \\ T_{dl} = \frac{1}{2}\left(J_e\dot{\omega} + \frac{F_R R_w}{\eta G}\right) - \frac{R_w}{t_{w1}\eta G}(I_z \cdot \dot{r} - (F_{yfl} + F_{yfr}) \\ \quad \cos\delta a + (F_{yrl} + F_{yrr})b - (T \cdot R - F_r)\sin\delta a). \end{cases} \quad (22)$$

B. Predictive Speed-Tracking Control Method

The theoretical distributed load has the derivation of the yaw rate r and lateral tire force F_{yi} which does not actually exist in the HIL test. It is hard to estimate in the real time. The predictive speed-tracking control method is proposed to generate the equivalent dynamic distributed load for DEP. The basic idea of the speed-tracking method for bench control is that it makes that the DEP on bench operates at the same rotation speed as the one equipped on the vehicle in the real road test.

The speed-tracking method is shown in Fig. 6. VCU's torque distribution command ($\bar{T}_{el}$ and $\bar{T}_{er}$) are received simultaneously by the real-time system and the MCU of DEP. The DVRRT model mentioned above predicts the rotation speed of each individual motor shaft in the next sample time. The predictive speed is used as a reference speed for the dynamometer speed control. Since the test bench structure is completely symmetrical, it is only necessary to analyze the
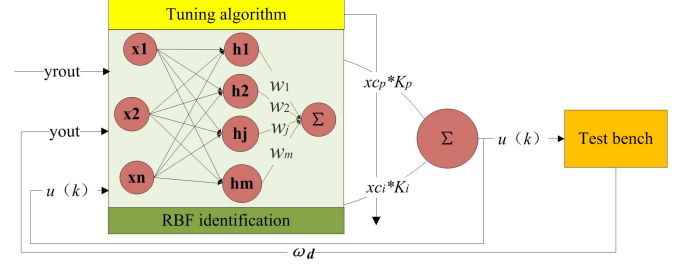

Fig. 7. Structure of SNPI controller with RBF identification (SNPI-RBF).

bench dynamics of one side. The rotational inertia of DM and dynamometer are J_m and J_d. ω_m and ω_d are the rotation speed. T_m and T_d are the electric torques. K and D are the stiffness and damping of the whole shaft and coupling module. Torque transmitted on the shaft is T_{shaft} which is detected by sensors as T_{sensor}.

C. Single-Neuron PI Control Method With Radial Basis Function Identification

1) Structure of Single-Neuron PI Controller: The dynamometer is a permanent magnet synchronous motor (PMSM) which is nonlinear, and the DEP torque output can be regarded as an interference for dynamometer speed control. A PI controller is established, in which PI gains are tuned online by a single neuron based on the radial basis function (RBF) network identification. The control method is stable, robust, and real time, which meet the requirements of the speed-tracking control.

The single-neuron PI (SNPI) controller combines the artificial neuron with the traditional PI controller. The structure of the SNPI controller was introduced in detail in [21]. The input of the proportional section xc_p is the speed error $e(k)$, while the integral section input xc_i is the integration of $e(k)$ where *ts* is the sample time, shown as

$$\begin{cases} xc_p(k) = e(k) \\ xc_i(k) = \sum_{k=1}^{k} ts \cdot e(k). \end{cases} \quad (23)$$

The structure of the SNPI controller is shown in Fig. 7. The single-neuron controller tunes the PI gains dynamically which is stated in the following equation:

$$\begin{cases} E = \frac{1}{2}e(k)^2 = \frac{1}{2}(y\text{rout}(k) - y\text{out}(k))^2 \\ \Delta K_p(k) = -\eta\frac{\partial E}{\partial K_p} = -\eta\frac{\partial E}{\partial y}\frac{\partial y}{\partial u}\frac{\partial u}{\partial K_p} = \eta e(k)\frac{\partial y}{\partial u}xc_p(k) \\ \Delta K_i(k) = -\eta\frac{\partial E}{\partial K_i} = -\eta\frac{\partial E}{\partial y}\frac{\partial y}{\partial u}\frac{\partial u}{\partial K_i} = \eta e(k)\frac{\partial y}{\partial u}xc_i(k) \\ u(k) = K_p(k)xc_p(k) + K_i(k)xc_i(k) \end{cases} \quad (24)$$

where $u(k)$ is the control output. K_p and K_i are the PI gains as well as the weights of neuron inputs. η is the learning rate. Excessive error input $e(k)$ causes the tuning algorithm not to converge. As a result, when the speed error $e(k)$ is larger than 10 r/min, the online tuning iteration is locked, and the PI gains K_p and K_i are directly inherited.

2) RBF Neuron Network Identification: The RBF neuron network introduced in [22] and [23] is used to identify dy/du. RBF defines a scalar function that describes the nonlinearity of a low-dimensional system by the Euclidean distance from any point in a multidimensional space to a given center. The input vector is X. The radial basis vector of a N-D input with M-D hidden layer network is H.

h_j is the Gaussian function that identifies the j node of the network hidden layer as

$$\begin{cases} X = [x_1 \quad x_2 \quad \cdots x_n]^{\mathrm{T}} \\ H = [h_1 \quad \cdots h_j \quad \cdots h_m]^{\mathrm{T}} \\ h_j = \exp\left(-\frac{\|X - C_j\|^2}{2b_j^2}\right) \\ C_j = [c_{j1} \quad \cdots c_{ji} \quad \cdots c_{jn}]^{\mathrm{T}} \end{cases} \quad (25)$$

where b_j is the base width of the j node. C_j is the center co-ordinate of the j node.

Hidden layer base-width vector is B. The weight vector of output layer is W. The output of the RBF network is y_m. The performance index evaluation function for network iterative learning is J_j, as

$$\begin{cases} B = [b_1 \quad b_2 \quad \cdots b_m]^{\mathrm{T}} \\ W = [w_1 \quad w_2 \quad \cdots w_m]^{\mathrm{T}} \\ y_m(k) = w_1 h_1 + w_2 h_2 + \cdots + w_m h_m \\ J_j = \frac{1}{2}(y\text{out}(k) - y_m(k))^2. \end{cases} \quad (26)$$

B, C_j, and W are iteratively updated according to a gradient descent learning algorithm, as

$$\begin{aligned} w_j(k) = w_j(k-1) &+ \eta_{\text{rbf}}(y\text{out}(k) - y_m(k))h_j \\ &+ \alpha(w_j(k-1) - w_j(k-2)) \end{aligned} \quad (27)$$

$$\begin{cases} \Delta b_j = (y\text{out}(k) - y_m(k))w_j h_j \dfrac{\|X - C_j\|^2}{b_j^3} \\ b_j(k) = b_j(k-1) + \eta_{\text{rbf}}\Delta b_j + \alpha(b_j(k-1) - b_j(k-2)) \\ \Delta c_{ji} = (y\text{out}(k) - y_m(k))w_j \dfrac{x_j - C_{ji}}{b_j^2} \\ c_{ji}(k) = c_{ji}(k-1) + \eta_{\text{rbf}}\Delta c_{ji} + \alpha(c_{ji}(k-1) - c_{ji}(k-2)). \end{cases} \quad (28)$$

The learning rate η_{rbf} ranges from 0 to 1. Inherited coefficient α ranges from 0 to 1. Identification of the test bench system Jacobian matrix is shown as

$$\frac{\delta y(k)}{\delta u(k)} \approx \frac{\delta y_m(k)}{\delta u(k)} = \sum_{j=1}^{m} \frac{\delta w_j h_j}{\delta u(k)} = \sum_{j=1}^{m} w_j h_j \frac{c_{ji} - x_1}{b_j^2} \quad (29)$$

D. Maximum Adhesion Limitation

The maximum adhesion of the road surface is the maximum load that the test bench should provide. Exceeding this torque, the tire starts sliding, and the vehicle becomes unstable. Unlike single-motor powertrain test, DEP test bench requires the precise determination of the maximum adhesion of each drive wheel. The maximum adhesion of each tire $F_{xi-\max}$ depends
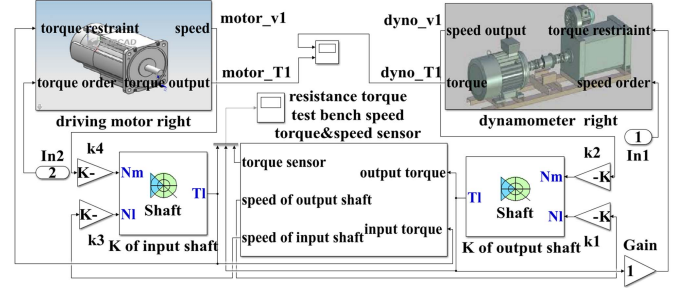

Fig. 8. Physical simulation model of DEP test bench in Simulink.

on the distribution of vertical loads F_{zi} and adhesion ratio. It is calculated according to

$$F_{xi-\max} = \mu F_{zi} \quad (30)$$

where μ is the adhesion coefficient.

When the wheel begins to slide, the rotation speed of each wheel changes fast, and the rotation speed of the wheel and DEP does not have a definite relationship with the vehicle speed. The inertia of them should be emulated by the test bench, with a special concern. The speed-tracking control method cannot generate the dynamic load accurately with the rapidly changing speed reference. As a result, the maximum adhesion saturation function is added to the dynamic load control algorithm. Dynamic relations as in (31) are always existed in the sliding process. Assuming that the DEP transmission on each side is a single-stage gearbox which transmission ratio is G, there are two parts in the DEP driveline with different rotation speeds. One part rotates at low speed ϖ_1 and inertia J_1, including wheel, half-shaft, and driven gear. Another part rotates at high speed ϖ_2 and inertia J_2, including input shaft and drive gear

$$\begin{cases} J_1 \dot{\varpi}_1 = T_1 - F_{xi-\max} R_w \\ T_{\text{load1}} = -\dfrac{T_1}{G} \\ J_2 \dot{\varpi}_2 = T_2 - T_{\text{load1}} \\ \dot{\varpi}_2 = G \dot{\varpi}_1. \end{cases} \quad (31)$$

The threshold value of the maximum adhesion saturation function is T_{load} as

$$T_{\text{load}} = \left(\frac{J_1}{G^2} + J_2\right)\dot{\varpi} + \frac{F_{xi-\max} R_w}{G}. \quad (32)$$

V. Simulation and Experiment of DEP Test Bench Under Conditions

A. Simulation Model for DEP Test Bench

The proposed DEP test bench and the control method are established and simulated. Simulation model is shown in Fig. 8.

The parameters of the vehicle and the test bench are shown in Tables I–III. The simulation conditions include a double-lane change (DLC) with constant speed reference (20 km/h), sliding condition during a steering maneuver on the bisectional roads, and a typical driving cycle condition.

<div style="display:flex">
<div>

TABLE I
SIMULATION PARAMETERS FOR DVRRT
MODEL IN SIMULINK

Name	symbol	value	unit
Vehicle model parameters			
DM inertia	J_m	0.042	kg·m^2
Vehicle mass	m	2100	kg
CG to front axle distance	a	1.256	m
CG to rear axle distance	b	1.368	m
Wheelbase	l	2.624	m
Front/rear track	tw	1.65	m
Yaw moment of inertia	I_z	2549	kg·m^2
Wheel rotation inertia	I_w	2.1	kg·m^2
CG height	hg	0.7	m
Wheel radius	R	0.31	m
Equivalent rolling radius	R_w	0.308	m
Rolling friction coefficient	f	0.013	-
Wind resistance coefficient	Cd	0.316	-
Frontal area	A	2.22	m^2
Dugoff tire model parameters			
Road friction coefficient	μ	0.4	-
Tire longitudinal stiffness	C_{xi}	50000	N/rad
Tire lateral stiffness	C_{yi}	30000	N/rad
Transmission parameters			
Part 1 inertia	J_1	2.102	kg·m^2
Part 2 inertia	J_2	0.0015	kg·m^2
Gear ratio	G	6.2	-

</div>
<div>

TABLE II
SIMULATION PARAMETERS OF THE TEST BENCH
PHYSICS MODEL IN SIMULINK

Name	symbol	value	unit
DM inertia	J_m	0.042	kg·m^2
Dynamometer inertia	J_d	0.042	kg·m^2
Damping coefficient	D	0.005	-
Stiffness of module	K	14550	Nm/rad

TABLE III
SNPI-RBF CONTROL PARAMETERS

Name	value	
Initial PI	$K_p=5$	$K_i=20$
PI range	K_p: $\begin{bmatrix}0 & 50\end{bmatrix}$	K_i: $\begin{bmatrix}0 & +\propto\end{bmatrix}$
Initial B of RBF	$\begin{bmatrix}5.3074 & 1.4771 & 26.4114 & 22.1716 & 52.9082 & 5.6906\end{bmatrix}^T$	
Initial C of RBF	$\begin{bmatrix}-3.1829 & -0.5211 & 7.1754 & 11.6631 & -3.6992 & -10.9150 \\ -3.8909 & 2.3999 & 5.1730 & 8.5871 & -11.3737 & -7.0179 \\ -4.2018 & 2.6742 & 5.1828 & 8.5238 & -1.8936 & -6.1845\end{bmatrix}$	
Initial W of RBF	$\begin{bmatrix}-0.5646 & 0.3937 & -0.5556 & 0.3981 & 0.4495 & 0.2565\end{bmatrix}^T$	
$\eta=0.8$ $\eta_{rbf}=0.4$ $\alpha=0.05$ n=3 m=6		

</div>
</div>

B. Simulation Results

1) DLC Condition: The simulation result is shown in Fig. 9. The test bench physics model including PMSM block provided in MATLAB/Simulink is used. The proposed SNPI-RBF controller is compared with another advanced PMSM speed control algorithm [24] which uses the sliding mode control (SMC) method. The given path and the trajectory are shown in Fig. 9(a). The maximum lateral deviation is 0.25 m. The driver model generates an appropriate steering angle during this process. Both the steering angle and the longitudinal/lateral displacement are shown in Fig. 9(b). The proposed DVRRT model is proven to provide a suitable real-time DLC working condition for the DEP in the loop.

The physics model of the test bench is controlled by the proposed dynamic loading method. In Fig. 9(c), the simulated speeds of dynamometers controlled by different methods (SMC and SNPI-RBF) are compared with the theoretical speed of the distributed DMs. The predictive speed-tracking control method shows a good performance which makes the distribute DM under test work at the actual speed in ground test. Compared with the SMC method, the SNPI-RBF method shows an advantage in reducing speed fluctuation. In Fig. 9(d), the dynamic loads generated by the dynamometers controlled by different methods are compared with the theoretical DEP loads calculated by (22). Dynamic loads of the SNPI-RBF method can track theoretical values, but dynamometers' torque output has 1-Nm ripple. In contrast, the SMC method cannot generate the accurate dynamic load. In SNPI-RBF, the PI gains are tuned by the single-neuron online, as shown in Fig. 9(e), the tuning tendency conforms to the theory, in which the optimal integrate gain K_I is related to PMSM speed and the proportion gain K_P keep increasing and converge gradually during the process. The RBF identification of the test bench system gain dy/du is also shown in Fig. 9(e).

2) Sliding Condition: In order to verify if the test bench can generate the accurate dynamic load under sliding conditions, the road is set as a bisectional road, in which the ground adhesion coefficient of the left side is reduced from 0.4 to 0.03 at the range of 40–80 m, as shown in Fig. 10(a). In this case, one driving wheel's tire force exceeds the maximum adhesion during the cornering process, and that wheel begins to slide. An antisliding control method is added to the torque
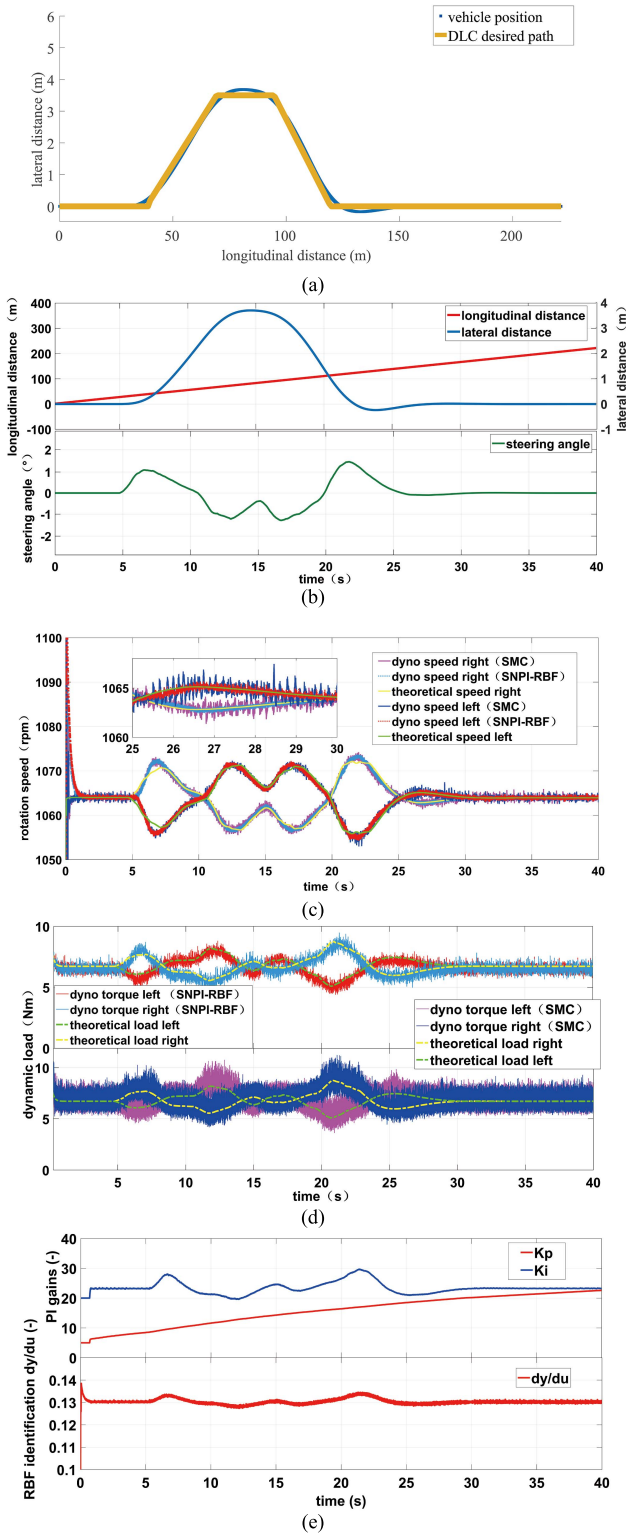
Fig. 9. Simulation results for the DEP test bench under DLC condition. (a) Track. (b) Longitudinal/lateral displacement and steering angle of front wheels. (c) Speed of the dynamometers on DEP test bench. (d) Dynamic load generated by the dynamometers. (e) PI gains of test bench controller and RBF identification results.

Fig. 10. Simulation results for the DEP test bench under sliding condition. (a) Steering maneuver on a bisectional road. (b) Speed of the DMs equipped on the driving wheels. (c) Load of the DMs equipped on the driving wheels. (d) Maximum adhesion limitation and each component of the load.

distribution algorithm of VCU which keeps the slip ratio under 0.2. The proposed maximum adhesion limitation of the bench control strategy is enabled under this condition. Simulation results are also shown. In Fig. 10(b), the simulated bench
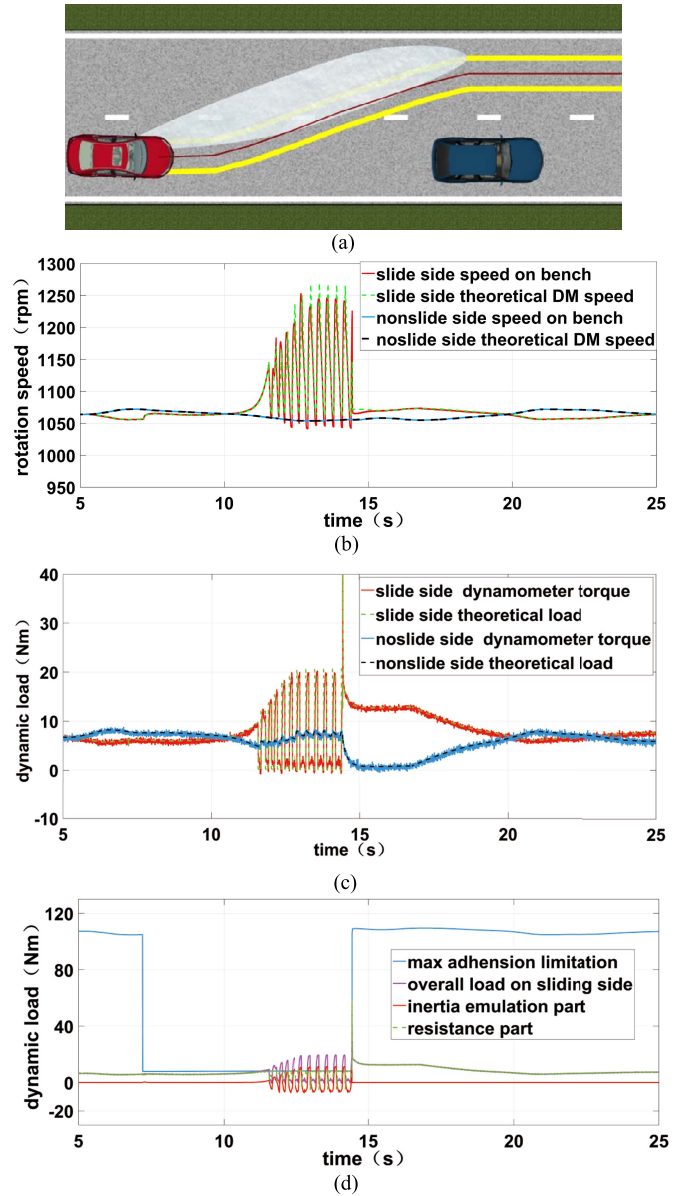
speed follows the theoretical speed of the DM under sliding condition. The speed error of the proposed test bench control method is 1%. In Fig. 10(c), the dynamic load generated by the dynamometer is equal to the theoretical load on the DM under the sliding condition, loading accuracy is 1.5 Nm, with ±2-Nm torque ripple. When the tire drives from the low adhesion surface to the high adhesion surface, the sliding wheel decelerates dramatically. It causes the peak of the DM load shown in Fig. 10(c). The whole sliding process of DEP is emulated on the test bench. Fig. 10(d) shows the maximum adhesion limitation during the whole process, the overall load acts on the sliding-side DM and the individual parts of the dynamometer torque command corresponding to (32) (inertia emulation part: $((J_1/G^2) + J_2)\dot{\varpi}$ and resistance part: $(F_{xi-\max} R_w/G)$). The resistance part is limited by the maximum adhesion.
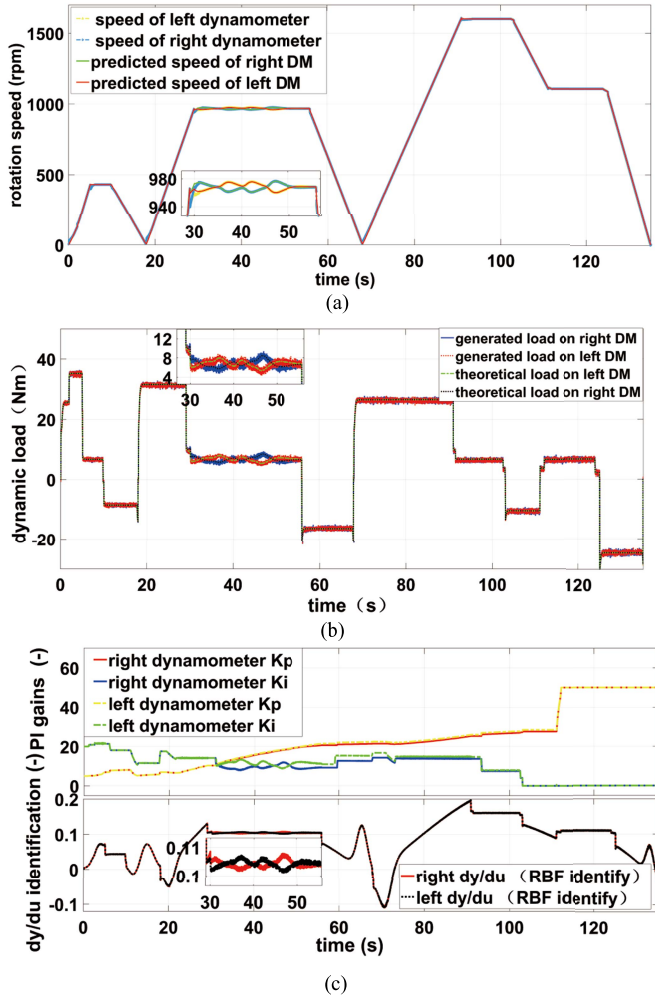
Fig. 11. Simulation results for the DEP test bench under driving cycle. (a) Speed of the dynamometers on the DEP test bench. (b) Dynamic load generated by the dynamometers. (c) PI gains of test bench controller and RBF identification results.
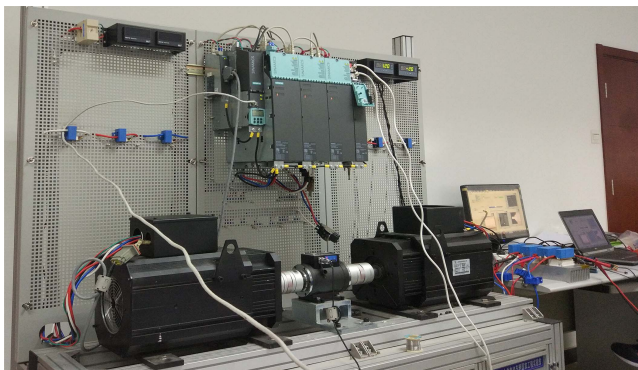

Fig. 12. One side of the experiment DEP test bench.

The simulation result shows that the maximum adhesion limitation in the test bench control method can generate the accurate dynamic load under sliding conditions.

3) Driving Cycle Condition: Considering the general work condition of the DEP, a driving cycle attached with lane changes from 28 to 55 s is set as the work condition. The simulation results are shown in Fig. 11. The bench speed and the dynamic load generated by the dynamometers match the
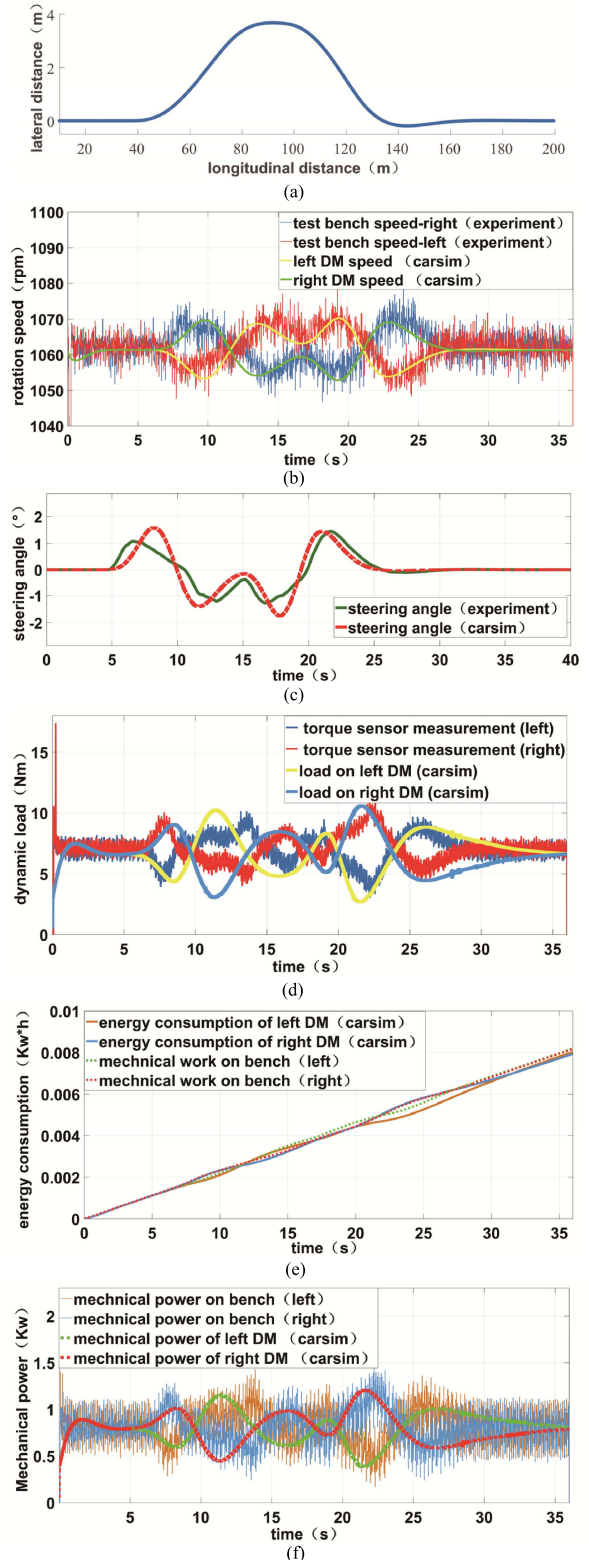

Fig. 13. Comparison of the experiment results and Carsim simulation results with the same DLC process. (a) Track. (b) Rotation speed of test bench. (c) Steering inputs of different driver models. (d) Dynamic load output of the DEP test bench. (e) Mechanical work. (f) Instantaneous mechanical power.

theoretical speed and load of two independent DMs during the entire cycle. The PI gains are tuned online to adapt the dynamic work condition, as shown in Fig. 11(c). During the differential steering process, the conditions of two independent

DMs are different, and the optimal PI gains are tuned differently. When the speed drops dramatically, K_i decreases to 0, and K_p increases to the maximum value, PI control degenerates into the proportional control. RBF identification of dy/du during the whole cycle is also shown. The result shows the proposed neuron PI speed-tracking test bench control method can provide a virtual real-time testing environment for DEP on bench. Under different work conditions, dy/du of the bench system is identified by the RBF neuron network, and PI gains are tuned online.

C. Experiment

1) Test Bench: Fig. 12 shows one side of the experiment DEP test bench controlled by the proposed speed-tracking method, including two PMSMs working as dynamometer and DM, respectively.

The same vehicle dynamic process (DLC) is implemented by the cosimulation of MATLAB/Simulink and Carsim to replace the ground test experiment and get the real dynamic load on each DM during the DLC condition, which is used to verify the generated load.

2) Results Analysis: The experiment results are shown in Fig. 13. The DLC trajectory of the DVRRT model running in the test bench control real-time system is shown in Fig. 13(a). In Fig. 13(b), the experiment rotation speed of the DMs under test (measured by the rotary encoder) is compared with each DM's rotation speed (cosimulation). The results verify that the DEP tested on bench is under the equal speed with the one in the real road test during the DLC process, and the speed control accuracy is up to 98%. The steering angles given by the Carsim driver model and the DVRRT's driver model are compared in Fig. 13(c). The longitudinal force on each tire during the DLC process is obtained by the Simulink/Carsim cosimulation, and converts to the load (torque) on each DM. The generated load which is measured by the torque sensor on the bench is compared with it shown in Fig. 13(d). Matching these two curves and analyzing the corresponding feature points, the overlap ratio of the two loads is over 93% with a time delay. The difference between the simulation load and experimental measurement is mainly caused by different steering angle input given by the driver model in Carsim and proposed DVRRT model. To do the efficiency test for DEP, the accuracy of the energy consumption measurement is important. In Fig. 13(e), the experiment mechanical work of the two independent DMs of DEP is 0.00815 and 0.0082 Kw·h, respectively. The mechanical energy consumption of DMs (cosimulation) is 0.00795 and 0.0080 Kwh, respectively. The measured mechanical energy is accurate (97.5%, the error between the measured one and the theoretical value is less than 2.5%). The instantaneous mechanical power is also shown and compared in Fig. 13(f), the measurement instantaneous mechanical power is unstable because of the ripples of the dynamometers' speed and torque output [25].

VI. CONCLUSION

A novel control method is proposed for the DEP test bench. It provides a real-time dynamic load for each DM

of DEP. Based on the novel bench structure, the equivalent load is generated by the DVRRT model speed prediction and dynamometers' speed-tracking control method. The maximum adhesion limitation and RBF identification neuron PI for dynamometer control are illustrated. Vehicle dynamics and the theoretical dynamic load of the DEP is calculated and compared with the generated real-time load of the proposed method. Simulations and experiment are done to verify the performance of the proposed speed-tracking control method and draw the following conclusion.

1) A virtual test environment is created by the proposed control method. The dynamic load and rotation speed of the independent DMs of DEP are equal to the theoretical one in the real road test. The dynamometers' speed control method is effective with a high accuracy, and the dynamic distribute loads are precisely emulated by the test bench. A ripple and time delay exist in the dynamometer output both in simulation and experiment, which depends on the torque response of dynamometers.

2) Some typical driving conditions of the DEP including steering maneuvers, sliding, and driving cycle can be reproduced and tested. The dynamometers' control parameters (PI gains) can be tuned online by the neuron based on the RBF identification to optimize the dynamometers' response performance.

In the future, the principle between the time delay of the real-time dynamic loading and the control strategy of the test bench will be studied. The experimental comparison of different dynamometers' speed controllers will be done.

REFERENCES

[1] Ž. Hederic, M. Hadžiselimovic, and B. Štumberger, "Modeling of a serial hybrid powertrain for busses in the city of Osijek, Croatia," in *Proc. IEEE Int. Energy Conf. (ENERGYCON)*, Cavtat, Croatia, May 2014, pp. 1537–1543.

[2] H. A. Yavasoglu, J. Shen, C. Shi, M. Gokasan, and A. Khaligh, "Power split control strategy for an EV powertrain with two propulsion machines," *IEEE Trans. Transport. Electrific.*, vol. 1, no. 4, pp. 382–390, Dec. 2015.

[3] M. Hu, J. Zeng, S. Xu, C. Fu, and D. Qin, "Efficiency study of a dual-motor coupling EV powertrain," *IEEE Trans. Veh. Technol.*, vol. 64, no. 6, pp. 2252–2260, Jun. 2015.

[4] L. Zhai, R. Hou, T. Sun, and S. Kavuma, "Continuous steering stability control based on an energy-saving torque distribution algorithm for a four in-wheel-motor independent-drive electric vehicle," *Energies*, vol. 11, no. 2, p. 350, 2018.

[5] K. Maeda, H. Fujimoto, and Y. Hori, "Four-wheel driving-force distribution method based on driving stiffness and slip ratio estimation for electric vehicle with in-wheel motors," in *Proc. IEEE Vehicle Power Propuls. Conf.*, Oct. 2012, pp. 1286–1291.

[6] G. De Filippis, B. Lenzo, A. Sorniotti, K. Sannen, J. De Smet, and P. Gruber, "On the energy efficiency of electric vehicles with multiple motors," in *Proc. IEEE Vehicle Power Propuls. Conf.*, Oct. 2016, pp. 1–6.

[7] P. Gao, Y. Gu, and X. Wang, "The design of a permanent magnet in-wheel motor with dual-stator and dual-field-excitation used in electric vehicles," *Energies*, vol. 11, no. 2, p. 424, 2018.

[8] Y. U. Zhuoping, F. Yuan, and X. Lu, "Review on vehicle dynamics control of distributed drive electric vehicle," *J. Mech. Eng.*, vol. 49, no. 8, pp. 105–114, 2013.

[9] B. Bilgin *et al.*, "Making the case for electrified transportation," *IEEE Trans. Transport. Electrific.*, vol. 1, no. 1, pp. 4–17, Jun. 2015.

[10] *Drive Motor System for Electric Vehicles—Part 2: Test Methods*, National Standard of China GB/T 18488.2-2015, 2015.

[11] R. W. Newton, R. E. Betz, and H. B. Penfold, "Emulating dynamic load characteristics using a dynamic dynamometer," in *Proc. Int. Conf. Power Electron. Drive Syst.*, vol. 1, Feb. 1995, pp. 465–470.

[12] C. Ma, M. Xu, and H. Wang, "Dynamic emulation of road/tyre longitudinal interaction for developing electric vehicle control systems," *Vehicle Syst. Dyn.*, vol. 49, no. 3, pp. 433–447, 2011.

[13] P. Fajri, V. A. K. Prabhala, and M. Ferdowsi, "Emulating on-road operating conditions for electric-drive propulsion systems," *IEEE Trans. Energy Convers.*, vol. 31, no. 1, pp. 1–17, Mar. 2016.

[14] P. Fajri, S. Lee, V. A. K. Prabhala, M. Ferdowsi, "Modeling and integration of electric vehicle regenerative and friction braking for motor/dynamometer test bench emulation," *IEEE Trans. Veh. Technol.*, vol. 65, no. 6, pp. 4264–4273, Jun. 2016.

[15] J. Park, H. Jeong, I. G. Jang, and S. H. Hwang, "Torque distribution algorithm for an independently driven electric vehicle using a fuzzy control method," *Energies*, vol. 8, no. 8, pp. 8537–8561, Aug. 2015.

[16] W. Zhao *et al.*, "Distributive electric powertrain system HIL modeling and test bench simulation based on preview driver model," *J. Beijing Inst. Technol. (English Ed.)*, vol. 26, pp. 59–66, Dec. 2017.

[17] H. Ding, K. Guo, F. Li, and W. Zhang, "Arbitrary path and speed following driver model based on vehicle acceleration feedback," *J. Mech. Eng.*, vol. 46, no. 10, pp. 116–120, 2010.

[18] T. Wilhelem, H. Okuda, B. Levedahl, and T. Suzuki, "Energy consumption evaluation based on a personalized driver–vehicle model," *IEEE Trans. Intell. Transp. Syst.*, vol. 18, no. 6, pp. 1468–1477, Jun. 2017.

[19] S. Qiang and L. Lin, "Mechanical decoupling algorithm applied to electric drive test bed," *Math. Problems Eng.*, vol. 2014, Aug. 2014, Art. no. 710865.

[20] W. Liu *et al.*, "A novel driver model for real-time simulation on electric powertrain test bench," in *Proc. Int. Powertrains, Fuels Lubricants Meeting*, 2017, pp. 1–8.

[21] W. Zhao, Q. Song, and Y. Huang, "A novel decoupling control method based on neural network for EV's Driving PMSM," in *Proc. CMSME*, Beijing, China, 2018, pp. 1–7. [Online]. Available: https://dx.doi.org/10.1088/1757-899X/383/1/012038

[22] J.-W. Perng, G.-Y. Chen, and S.-C. Hsieh, "Optimal PID controller design based on PSO-RBFNN for wind turbine systems," *Energies*, vol. 7, no. 1, pp. 191–209, 2014.

[23] I. Poultangari, R. Shahnazi, and M. Sheikhan, "RBF neural network based PI pitch controller for a class of 5-MW wind turbines using particle swarm optimization algorithm," *ISA Trans.*, vol. 51, no. 5, pp. 641–648, 2012.

[24] W. Xiangrui and G. Jian, "Permanent magnet synchronous motor sliding mode control by MATLAB simulation," *Electron. Des. Eng.*, vol. 25, no. 11, 2017.

[25] Q. Song, Y. Li, and C. Jia, "A novel direct torque control method based on asymmetric boundary layer sliding mode control for PMSM," *Energies*, vol. 11, no. 2, p. 657, 2018.

Qiang Song received the Ph.D. degree in mechanical engineering from the Beijing Institute of Technology (BIT), Beijing, China, in 2004.

From 2004 to 2008, he was a Lecturer with BIT, where he has been an Associate Professor since 2008. He designed the first special test bench for EV's driving motor (DM) in China. He also leads a research team which was including four Chinese national key laboratories to do research on the key components of EV DM system like insulated-gate bipolar transistor (IGBT)/film capacitor/current sensor/magnetic material/silicon steel, as well as the whole system of the motors. His current research interests include design, control, and optimization of powertrain system and energy storage unit of electric vehicle (EV).

Wenbin Liu was born in Lu'an, China, in 1995. He is currently pursuing the M.S. degree in mechanical engineering with the Beijing Institute of Technology, Beijing, China.

He focuses on research and development of electric powertrain hardware-in-the-loop (HIL) testing system.

Mukhtiar Ahmad was born in Dera Ghazi Khan, Pakistan, in 1989. He is currently pursuing the Ph.D. degree with the School of Mechanical Engineering, Beijing Institute of Technology, Beijing, China.

His current research interests include hardware-in-the-loop (HIL) technology of electric powertrain system, DEP's HIL test bench, and dynamic loading.

Wanbang Zhao was born in Mudanjiang, China, in 1992. He received the B.S. degree in vehicle engineering from the Dalian University of Technology, Dalian, China, in 2016. He is currently pursuing the M.S. degree in mechanical engineering.

In 2019, he joined SAIC Motor. Since 2016, he has been a Researcher with the National Engineering Laboratory for Electric Vehicles, Beijing Institute of Technology, Beijing, China. His current research interests include electric powertrain hardware-in-the-loop (HIL) testing technology, dynamics of distributed driving electric vehicles (EVs), and electric motor control.

Yiting Li was born in Shandong, China, in 1992. He is currently pursuing the Ph.D. degree in mechanical engineering with the Beijing Institute of Technology, Beijing, China.

His current research interests include electric motor vehicle high-efficiency motor control.